CILP1 as a biomarker for right ventricular maladaptation in pulmonary hypertension

Stanislav Keranov[1,2], Oliver Dörr[1,2], Leili Jafari[3], Christian Troidl[2,3], Christoph Liebetrau[1,2,3], Steffen Kriechbaum[3], Till Keller[2,3], Sandra Voss[3], Timm Bauer[1], Jakob Lorenz[1], Manuel J. Richter[4], Khodr Tello[4], Henning Gall[4], Hossein A. Ghofrani[4], Eckhard Mayer[5], Christoph B. Wiedenroth[5], Stefan Guth[5], Holger Lörchner[6], Jochen Pöling[6], Prakash Chelladurai[6], Soni Savai Pullamsetti[6], Thomas Braun[6], Werner Seeger[4], Christian W. Hamm[1,2,3] and Holger Nef[1,2]

Affiliations: [1]University of Giessen, Dept of Cardiology and Angiology, Giessen, Germany. [2]DZHK (German Center for Cardiovascular Research), Partner Site RheinMain, Frankfurt am Main, Germany. [3]Kerckhoff Heart and Lung Center, Dept of Cardiology, Bad Nauheim, Germany. [4]Dept of Internal Medicine, Justus-Liebig-University Giessen, Universities of Giessen and Marburg Lung Center (UGMLC), Member of the German Center for Lung Research (DZL), Giessen, Germany. [5]Kerckhoff Heart and Lung Center, Dept of Thoracic Surgery, Bad Nauheim, Germany. [6]Max Planck Institute for Heart and Lung Research, Bad Nauheim, Germany.

Correspondence: Stanislav Keranov, Dept of Cardiology and Angiology, University of Giessen, Klinikstr. 33, 35392 Giessen, Germany. E-mail: stanislav.keranov@innere.med.uni-giessen.de

@ERSpublications
CILP1 is a novel biomarker of RV and LV pathological remodelling that is associated with RV maladaptation and ventriculoarterial uncoupling in patients with pulmonary hypertension
https://bit.ly/33HwLtN

Cite this article as: Keranov S, Dörr O, Jafari L, *et al*. CILP1 as a biomarker for right ventricular maladaptation in pulmonary hypertension. *Eur Respir J* 2021; 57: 1901192 [https://doi.org/10.1183/13993003.01192-2019].

ABSTRACT The aim of our study was to analyse the protein expression of cartilage intermediate layer protein (CILP)1 in a mouse model of right ventricular (RV) pressure overload and to evaluate CILP1 as a biomarker of cardiac remodelling and maladaptive RV function in patients with pulmonary hypertension (PH).

Pulmonary artery banding was performed in 14 mice; another nine mice underwent sham surgery. CILP1 protein expression was analysed in all hearts using Western blotting and immunostaining. CILP1 serum concentrations were measured in 161 patients (97 with adaptive and maladaptive RV pressure overload caused by PH; 25 with left ventricular (LV) hypertrophy; 20 with dilative cardiomyopathy (DCM); 19 controls without LV or RV abnormalities)

In mice, the amount of RV CILP1 was markedly higher after banding than after sham. Control patients had lower CILP1 serum levels than all other groups ($p<0.001$). CILP1 concentrations were higher in PH patients with maladaptive RV function than those with adaptive RV function ($p<0.001$), LV pressure overload ($p<0.001$) and DCM ($p=0.003$). CILP1 showed good predictive power for maladaptive RV in receiver operating characteristic analysis (area under the curve (AUC) 0.79). There was no significant difference between the AUCs of CILP1 and N-terminal pro-brain natriuretic peptide (NT-proBNP) (AUC 0.82). High CILP1 (cut-off value for maladaptive RV of $\geqslant 4373$ pg·mL^{-1}) was associated with lower tricuspid annular plane excursion/pulmonary artery systolic pressure ratios ($p<0.001$) and higher NT-proBNP levels ($p<0.001$).

CILP1 is a novel biomarker of RV and LV pathological remodelling that is associated with RV maladaptation and ventriculoarterial uncoupling in patients with PH.

This article has an editorial commentary: https://doi.org/10.1183/13993003.04277-2020

This article has supplementary material available from erj.ersjournals.com

Received: 17 June 2019 | Accepted after revision: 3 Oct 2020

Introduction

Pulmonary hypertension (PH) leads to pressure overload of the right ventricle (RV), which initially causes adaptive RV changes such as increased wall thickness and contractility. However, persistently increased afterload results in maladaptive pathological remodelling, ventriculoarterial uncoupling and right heart failure, changes that are associated with worse outcomes [1]. RV failure is one of the strongest predictors of mortality in PH [2].

Hence, it is important to develop diagnostic tools that are able to assess disease severity and detect early maladaptive changes in RV function and structure. Several studies have shown that biomarkers such as N-terminal pro-brain natriuretic peptide (NT-proBNP), troponin I, tissue inhibitor of metalloproteinase-1 and -2 and insulin growth factor binding protein-2 are associated with worse prognosis in patients with PH [3–5]. Additional research is needed to identify new biomarkers that can further improve the accuracy of diagnostic work-up. Moreover, there are currently no established biomarkers of pathological myocardial remodelling and myocardial fibrosis in particular.

Cartilage intermediate layer protein (CILP)1, an antagonist of transforming growth factor (TGF)-β, is an extracellular matrix (ECM) protein involved in profibrotic signalling in myocardium [6]. CILP1 RNA expression is upregulated in animal models of left ventricular (LV) pressure overload and LV myocardial infarction, and CILP1 protein levels were significantly elevated in myocardial tissue of patients with aortic stenosis or myocardial infarction [6, 7]. Interestingly, its expression at the RNA level in mouse models was shown to be more pronounced in RV pressure overload than in LV pressure overload [8].

The aim of this investigation was to analyse the expression of CILP1 under conditions of RV pressure overload and to determine its potential as a biomarker of pathological myocardial remodelling and RV maladaptation.

Methods

Mouse model of RV pressure overload: pulmonary artery banding

All animal experiments in this study were performed with approval of the university ethics committee for the care and use of laboratory animals and the local authorities (Regierungspräsidium Giessen). 9- to 10-week-old male C57/Bl6 mice (total of 23) were anaesthetised with inhaled 1.5–2.0% isoflurane, intubated and ventilated with oxygen. To induce reproducible pressure overload of the right ventricle, a constriction of the proximal pulmonary artery was applied. After upper left-sided thoracotomy, the outflow tract of the right heart was exposed, the pulmonary artery was dissected, and a Weck Hemoclip (Teleflex Incorporated, Wayne, PA, USA) was applied around the pulmonary artery, resulting in its constriction. The Hemoclip applicator had an adjuster bolt, allowing a precise, defined, partial closure of the clip. Mild banding (inner clip area of 1.25 mm^2) was performed in five mice; another nine mice underwent severe banding (inner clip area of 1.13 mm^2); and nine sham-operated controls underwent thoracotomy without banding. All animals were sacrificed 7 days after surgery.

Protein extraction and Western blot analysis

Proteins from RV tissue were isolated, and Western blot analysis was performed according to protocols described previously [9]. The following antibodies were used for Western blotting: CILP1 antibody (Biorbyt, Cambridge, UK; catalogue no. orb182643), atrial natriuretic peptide (ANP) antibody (Merck, Kenilworth, NJ, USA; catalogue no. AB5490), and pan-actin antibody (Cell Signaling Technology, Danvers, MA, USA; catalogue no. 4968).

Immunofluorescence

Tissue samples were characterised using haematoxylin and eosin staining (Chroma/Waldeck, Münster, Germany) according to standard protocols before immunostaining. Samples for fluorescence microscopy were processed as described previously [10]. The following antibodies were used for immunofluorescence staining: rabbit anti-collagen type 1 (Rockland Immunochemicals, Limerick, PA, USA; catalogue no. 600-401-103), rabbit anti-collagen type 3 (Rockland Immunochemicals; catalogue no. 600-401-105), and CILP antibody (Biorbyt; catalogue no. orb182643).

Immunofluorescence was assessed using ×40 Planapo objective (Leica, Wetzlar, Germany) and a Leica (Leitz DMRB) fluorescence microscope equipped with a Leica DC380 digital camera. Quantitative analysis was performed according to a previously described protocol using images analysis software (Leica) and the Image J programme [10]. The areas highlighted by different markers were calculated as percentage of the respective signal per tissue area.

Cell culture and treatments

Human adult cardiac fibroblasts were purchased from ScienCell Research Laboratories (Carlsbad, CA, USA), and maintained under normoxic conditions (21% oxygen) at 37°C in a humidified incubator with 5% carbon dioxide, according to the supplier's instructions. Importantly, poly-L-lysine (ScienCell Research Laboratories) was used as a coating agent (2 $\mu g \cdot cm^{-2}$) to promote cardiac fibroblast adhesion in culture. It was incubated for a minimum of 2 h at 37°C and removed before addition of fibroblasts media (basal fibroblast medium supplemented with 10 mL fetal bovine serum, 5 mL fibroblast growth supplement and 5 mL penicillin/streptomycin, provided by ScienCell) and cells to the flask. Cardiac fibroblasts between second to sixth passages were used for experiments. To determine the regulation of CILP1 and target genes, cardiac fibroblasts were seeded in six-well plates and stimulated with or without fetal bovine serum (2%), or TGF-β1 (5 $ng \cdot mL^{-1}$; Peprotech, London, UK) in basal fibroblast medium for 6, 48 and 72 h.

RNA extraction, cDNA synthesis and real-time PCR

Total RNA was harvested in RLT buffer (10 µL β-mercaptoethanol·mL^{-1} of RLT) and extracted from cardiac fibroblasts using the RNeasy Mini Kit (Qiagen, Hilden, Germany) according to the manufacturer's protocol. Genomic DNA was removed by on-column digestion with RNase-free DNase I (Qiagen). The quality and quantity of purified RNA was measured using NanoDrop 2000 Spectrophotometer (ThermoFisher Scientific, Waltham, MA, USA). The ratio of the readings at 260 nm and 280 nm (A260/A280) provides an estimate of the purity of RNA with respect to contaminants that absorb in the ultraviolet spectrum, such as protein. Pure RNA has an A260/A280 ratio of 1.9–2.1 (2.0). Complementary (c)DNA was synthesised from 1 µg of the total RNA using High Capacity cDNA synthesis kit (Applied Biosystems, Waltham, MA, USA), according to the manufacturer's protocol. Real-time PCR is widely used for quantification of mRNA levels for the genes of interest using C1000 Thermal Cycler (BioRad, Hercules, CA, USA) using iQ™ SYBR Green Supermix (Bio-Rad) according to the following protocol: initial denaturation for 5 min at 95°C with the number of repeats one; denaturation step with 40 cycles for 10 s at 95°C; annealing step for 15 s at 59°C with the number of repeats 40; elongation step at 72°C for 15 s and denaturation steps for 10 s at 95°C followed by a melt curve from 65°C to 95°C at 0.5°C increments for 3 s. Human-specific real-time PCR primers (table 1) were designed using Primer-BLAST (National Center for Biotechnology Information, Bethesda, MD, USA) and purchased from Metabion International (Munich, Germany). Gene expression was analysed using the Δ cycle threshold (Ct) method.

Human study population

From February 2014 to February 2018, 97 patients with chronic thromboembolic pulmonary hypertension (CTEPH) or idiopathic pulmonary arterial hypertension (IPAH), 25 with LV pressure overload resulting from severe aortic stenosis without RV abnormalities, 20 with dilative cardiomyopathy (DCM) without RV abnormalities, and 19 controls without LV or RV abnormalities (controls) were enrolled in this prospective study. Data on demographics, symptoms and comorbidities were collected for all patients. Baseline characteristics concerning LV and RV dimensions, function and pressure gradients were further evaluated by transthoracic echocardiography and right heart catheterisation.

TABLE 1 List of human primers for quantitative reverse-transcriptase PCR.

Gene name	Sequence (5′–3′)
HPRT	Forward: TGACACTGGCAAAACAAT Reverse: GGTCCTTTTCACCAGCAA
COL1A1	Forward: TTGGCACCAGGCAGACCAGCTTT Reverse: AAGCGAGGAGCTCGAGGTGAAC
COL1A2	Forward: TCTGCGACACAAGGAGTCTGT Reverse: GCTGGGCCCTTTCTTACAGT
COL3A1	Forward: TGGGAGAAATGGTGACCCTGGT Reverse: GGATAGCCTGCGAGTCCT
CILP1	Forward: AATTACACCGTACGCTTCCTCT Reverse: CATCTCTGCCAAGCAAATGC
POSTN	Forward: TGCCCAGCAGTTTTGCCCATT Reverse: CGTTGCTCTCCAAACCTCTA
FN1	Forward: AGCAGACCCAGCTTAGAGTTT Reverse: GCAGAAGTGTTTGGGTGACT
COL8A1	Forward: CTCACACGTTCACCAACTCAT Reverse: GGGCTGGTTTCTGTCTCTTCA

All patients provided written informed consent for their participation in the study, and approval of the institutional review board of the University of Giessen (99/13) was obtained. All participating PH patients were enrolled in the prospective Giessen PH Registry [11]. The investigation conforms to the principles outlined in the Declaration of Helsinki.

Laboratory assessment

Venous blood samples were collected in plain gel-filled tubes (Monovette; Saarstedt, Nümrecht, Germany) for the determination of CILP1 and NT-proBNP concentrations. Serum was processed immediately and frozen at −80°C until assay. CILP1 levels were determined using a high-sensitivity ELISA (human CILP1 ELISA kit, Cusabio Techology, Wuhan, China) with a detection range of 93.75–6000 $pg{\cdot}mL^{-1}$, a minimum detectable concentration of 23.4 $pg{\cdot}mL^{-1}$, an intra-assay precision coefficient of variation <8% and an interassay precision coefficient of variation <10%.

NT-proBNP levels were measured in serum with an electrochemiluminescence immunoassay using monoclonal antibodies (NT-proBNP assay; Roche Diagnostics, Mannheim, Germany). The intra-assay coefficients of variation are 1.5% and 1.3% at 124 and 14.142 $pg{\cdot}mL^{-1}$, respectively, and the respective interassay coefficients of variation are 2.7% and 1.7% at 125 and 32.930 $pg{\cdot}mL^{-1}$, respectively, as shown by the package insert. The lower detection limit for the NT-proBNP assay is 5 $pg{\cdot}mL^{-1}$.

Transthoracic echocardiography

All patients underwent transthoracic two-dimensional echocardiography using commercially available ultrasound systems (EPIQ 7: Philips Ultrasound Systems, Koninklijke Philips, Amsterdam, Netherlands; E9: General Electric, Boston, MA, USA; S5: General Electric). Left and right ventricular assessment was performed as recommended by recent guidelines [12].

Right heart catheterisation

Right heart catheterisation was performed *via* the right internal jugular vein using a 7F sheath and a standard Swan–Ganz catheter, as described previously [11, 13].

Classification of patients

Adaptive RV was defined as follows: preserved RV and LV function (tricuspid annular plane systolic excursion (TAPSE) >20 mm and LV ejection fraction (LVEF) >55%); cardiac index >2.5 $L{\cdot}min^{-1}{\cdot}m^{-2}$ despite chronic RV pressure overload with mean pulmonary artery pressure (PAP) ⩾25 mmHg) and no LV hypertrophy (end-diastolic interventricular septum thickness (IVSd) <12 mm, end-diastolic LV posterior wall thickness (LVPWd) <12 mm) in patients diagnosed with IPAH or CTEPH.

Maladaptive RV was defined as follows: RV failure (TAPSE <16 mm, cardiac index <2.2 $L{\cdot}min^{-1}{\cdot}m^{-2}$) and RV end-diastolic dilatation (>43 mm) caused by chronic RV pressure overload (mean PAP ⩾25 mmHg) in patients diagnosed with idiopathic PH or CTEPH, preserved LV function (LVEF >55%) and no LV hypertrophy (IVSd <12 mm, LVPWd <12 mm) in patients diagnosed with IPAH or CTEPH.

Patients with LV hypertrophy and pressure overload were included in the study according to the following criteria: chronic LV pressure overload due to severe aortic stenosis (aortic valve mean pressure gradient >40 mmHg and/or aortic valve area <1.0 cm^2), preserved RV function (TAPSE >20 mm) and preserved LV function (LVEF >55%), mean PAP <25 mmHg, RV end-diastolic basal diameter (RVD) <42 mm, IVSd ⩾12 mm and LVPWd ⩾12 mm.

Patients with DCM were included in the study according to the following criteria: preserved RV function (TAPSE >20 mm) and impaired LV function (LVEF <35%): mean PAP <25 mmHg amd RVD <42 mm.

Samples from a cohort without any right or left ventricular abnormalities were used as controls.

Statistical analysis

Continuous variables are presented as mean±SD or median (interquartile range (IQR)), as appropriate. Categorical variables are expressed as numbers and percentages. Parametric distribution was assessed with the Shapiro–Wilk test. Normally distributed continuous variables were compared using the Welch two-sample t-test and one-way analysis of variance with Bonferroni's *post hoc* test. The Mann–Whitney U-test and the Kruskal–Wallis test with Dunnett's *post hoc* test were used for non-normally distributed continuous variables. Receiver operating characteristic (ROC) curve analysis was performed to assess the predictive value of CILP1 regarding maladaptive RV pressure overload. The best CILP1 cut-off concentration for predicting maladaptive RV was then computed using the Youden index. Multivariable logistic regression analysis was used to identify independent predictors of CILP1 concentrations greater than or equal to the estimated cut-off (4373 $pg{\cdot}mL^{-1}$).

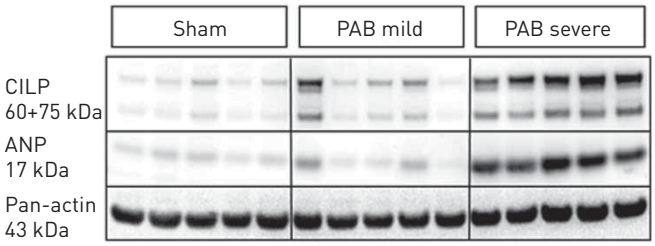

FIGURE 1 Western blot analysis of cartilage intermediate layer protein (CILP)1 and atrial natriuretic peptide (ANP) protein in murine right ventricle 1 week after sham, mild pulmonary artery banding (PAB) and severe PAB. Lanes show results from five different mice for each condition.

A two-tailed p-value <0.05 was considered to indicate statistical significance. Statistical analysis was performed using SPSS version 25 (SPSS, Chicago, IL, USA).

Results

Murine model of RV pressure overload and CILP1 expression

There was a significant increase in the RV weight and the ratio of RV weight/tibia length of mice subjected to severe pulmonary artery banding (PAB) compared with sham-operated animals (0.0025 g *versus* 0.0042 g for RV weight and 0.015 *versus* 0.025 for RV weight/tibia length ratio; p=0.03). All 23 animals operated survived until the end of the study.

Western blot analysis showed significantly higher amounts of CILP1 (figure 1, supplementary figure S1a) protein 1 week after severe PAB than after sham or mild PAB, which correlated with ANP protein levels (r=0.9, p=0.002) (figure 1, supplementary figure S1b). In addition, immunostaining revealed higher amounts of CILP1 after severe PAB (figure 2).

Tissue area measurements after immunostaining in hearts extracted from sham (n=4) and severe PAB (n=4) mice showed a markedly higher percentage of collagen type I and III in PAB than in sham animals (supplementary figure S2a and b).

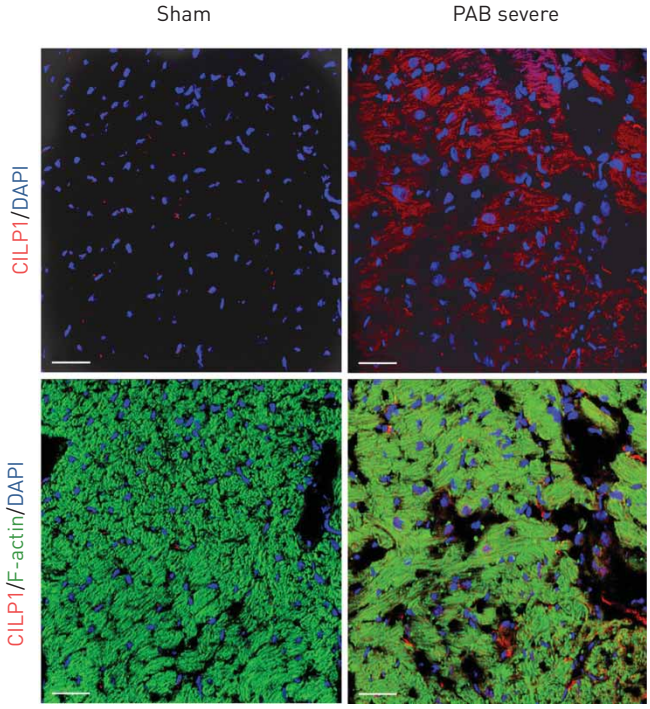

FIGURE 2 Immunofluorescence analysis of cartilage intermediate layer protein (CILP)1 in murine right ventricle 1 week after sham and severe pulmonary artery banding (PAB). CILP1 staining is shown in red. Nuclei were counterstained with 4′,6-diamidino-2-phenylindole (DAPI; blue) and F-actin was visualised with a specific antibody (green). Scale bars=30 μm.

CILP1 transcription in human cardiac fibroblasts

CILP1 transcription in human cardiac fibroblasts under serum-supplemented culture conditions was significantly lower than under basal medium after 6, 48 and 72 h (supplementary figure S3b). However, after TGF-β1 treatment, CILP1 transcription in human cardiac fibroblasts increased significantly at all time points as compared to basal medium (supplementary figure S3a). Periostin (POSTN) transcription was significantly higher after 48 and 72 h under TGF-β1 and serum, while fibronectin (FN)1 showed increased transcription only under TGF-β1 at 72 h (supplementary figure S3b). There was a trend towards higher COL1A2 transcription under TGF-β1 at 72 h (p=0.07) (supplementary figure S3b). In addition, there was a strong correlation between levels of CILP1, FN1, POSTN and COL1A2 at 72 h after TGF-β1 stimulation (supplementary figure S3c).

Characteristics of the human study population

Clinical and diagnostic characteristics of the entire study population (n=161) and the five groups are presented in table 2. The median (IQR) age was 67 (55–76) years and 48% of the patients were female.

Patients with adaptive RV showed higher values for mean PAP and end-diastolic RVD than patients with DCM (p<0.0001 for mean PAP, p<0.01 for RVD), LV hypertrophy (p<0.0001 for mean PAP, p<0.01 for RVD) and controls (p<0.001 for RVD; mean PAP was not measured), whereas there were no significant differences in TAPSE between adaptive RV, controls, DCM and LV hypertrophy. The cardiac index was lower in DCM and LV hypertrophy than in adaptive RV (p<0.0001 for adaptive RV *versus* DCM and LV hypertrophy).

Patients with maladaptive RV had a higher pulmonary artery systolic pressure (PASP), mean PAP and RVD as well as a lower TAPSE than those with adaptive RV (p<0.001 for mean PAP and PASP, p<0.0001 for RVD and TAPSE), DCM (p<0.0001 for PASP, mean PAP, RVD and TAPSE), LV hypertrophy (p<0.0001 for PASP, mean PAP, RVD and TAPSE) and controls (p<0.0001, for RVD and TAPSE; PASP and mean PAP not measured).

TABLE 2 Clinical characteristics

	All patients	Adaptive RV pressure overload	Maladaptive RV pressure overload	LV pressure overload	DCM	Control group
Patients	161	47	50	25	20	19
Female	77 (48)	26 (55)	27 (54)	14 (56)	5 (25)	5 (26)
Age years	67 (55–76)	64 (53–72)	60 (44–71)	82 (77–84)	59 (48–68)	75 (71–78)
BMI kg·m^{-2}	28 (25–31)	28 (24–32)	26 (22–29)	28 (25–31)	29 (25–34)	28 (25–30)
CAD	63 (51)	21 (68)	21 (66)	11 (44)	5 (25)	5 (31)
NYHA class ⩾III	41 (26)	8 (17)	13 (27)	15 (60)	2 (10)	3 (16)
Diabetes	41 (26)	12 (26)	12 (24)	12 (48)	3 (15)	2 (11)
Right heart catheterisation						
PASP mmHg	64 (37–88)	62 (51–78)	88 (75–101)	30 (28–35)	28 (24–32)	NA
Mean PAP mmHg	40 (24–55)	39 (32–49)	55 (47–63)	20 (18–24)	18 (16–21)	NA
Cardiac index L·min^{-1}·m^{-2}	2 (2–3)	3.04 (2.8–3.3)	1.75 (1.5–2.0)	2.1 (1.9–2.2)	1.6 (1.3–2.3)	NA
Mean PAWP mmHg	10 (8–13)	10 (7–12)	9 (8–12)	14 (8–18)	15 (10–21)	NA
RAP mmHg	8 (5–11)	5 (5–9)	11 (8–14)	6 (3–7)	6 (5–8)	NA
Echocardiography						
TAPSE mm	21 (16–24)	22 (21–26)	14 (12–16)	22 (20–25)	22 (20–26)	21 (20–22)
LVEF	60 (58–65)	63 (60–70)	62 (60–67)	65 (60–65)	33 (25–36)	60 (60–65)
RVD mm	41 (34–48)	40 (35–45)	50 (47–52)	31 (25–37)	38 (35–40)	29 (28–32)
IVSd mm	11 (9–12)	10 (9–11)	10 (9–11)	13 (12–14)	11 (10–13)	12 (11–12)
LVPWd mm	10 (9–12)	9 (8–10)	10 (9–11)	13 (12–13)	10 (9–11)	11 (10–11)
TAPSE/PASP mm·mmHg^{-1}	0.34 (0.17–0.59)	0.38 (0.29–0.49)	0.16 (0.13–0.21)	0.75 (0.59–0.96)	0.8 (0.67–0.98)	NA
CILP1 pg·mL^{-1}	3552 (2496–5538)	3544 (2727–4325)	5709 (4386–6341)	3189 (2484–3767)	3431 (2383–4980)	1389 (860–2214)
NT-proBNP pg·mL^{-1}	309 (100–996)	120 (49–324)	996 (306–1612)	253 (125–619)	632 (117–755)	NA

Data are presented as n, n (%) or median (interquartile range). RV: right ventricle; LV: left ventricle; DCM: dilative cardiomyopathy; BMI: body mass index; CAD: coronary artery disease; NYHA: New York Heart Association; PASP: pulmonary arterial systolic pressure; PAP: pulmonary artery pressure; PAWP: pulmonary artery wedge pressure; RAP: right atrial pressure; TAPSE: tricuspid annular plane systolic excursion; LVEF: left ventricular ejection fraction; RVD: right ventricular diameter; IVSd: diastolic interventricular septum thickness; LVPWd: diastolic left ventricular posterior wall thickness; CILP: cartilage intermediate layer protein; NT-proBNP: N-terminal pro-brain natriuretic peptide; NA: not applicable.

The clinical characteristics of the patients with adaptive CTEPH (47% of all adaptive RV patients) and IPAH (53% of all adaptive RV patients), as well as maladaptive CTEPH (26% of all maladaptive RV patients) and IPAH (63% all maladaptive RV patients) are shown in supplementary table S1. There were no significant differences in echocardiographic and right heart catheterisation parameters between adaptive CTEPH and adaptive IPAH or between maladaptive CTEPH and maladaptive IPAH.

Serum CILP1 and NT-proBNP levels

The median CILP1 concentrations in the whole cohort and in the separate groups are given in table 2 and shown in greater detail in figure 3. Patients with DCM, LV hypertrophy and PH (adaptive and maladaptive RV) had significantly higher CILP1 concentrations than the controls (figure 3a). There was no significant difference in CILP concentrations between DCM and LV hypertrophy (figure 3a). The adaptive RV group had higher CILP1 concentrations than the controls (figure 3b), but there was no difference between adaptive RV, LV hypertrophy, and DCM (figure 3c). Maladaptive RV patients had higher CILP1 concentrations than the controls (figure 3b) and those with LV hypertrophy and DCM (figure 3d). A direct comparison between the two RV groups revealed markedly higher CILP1 concentrations in the maladaptive group (figure 3b).

An association of higher CILP1 concentrations with maladaptive RV function was also evident in the subgroup analysis. There was a significant difference in CILP1 concentrations between adaptive and

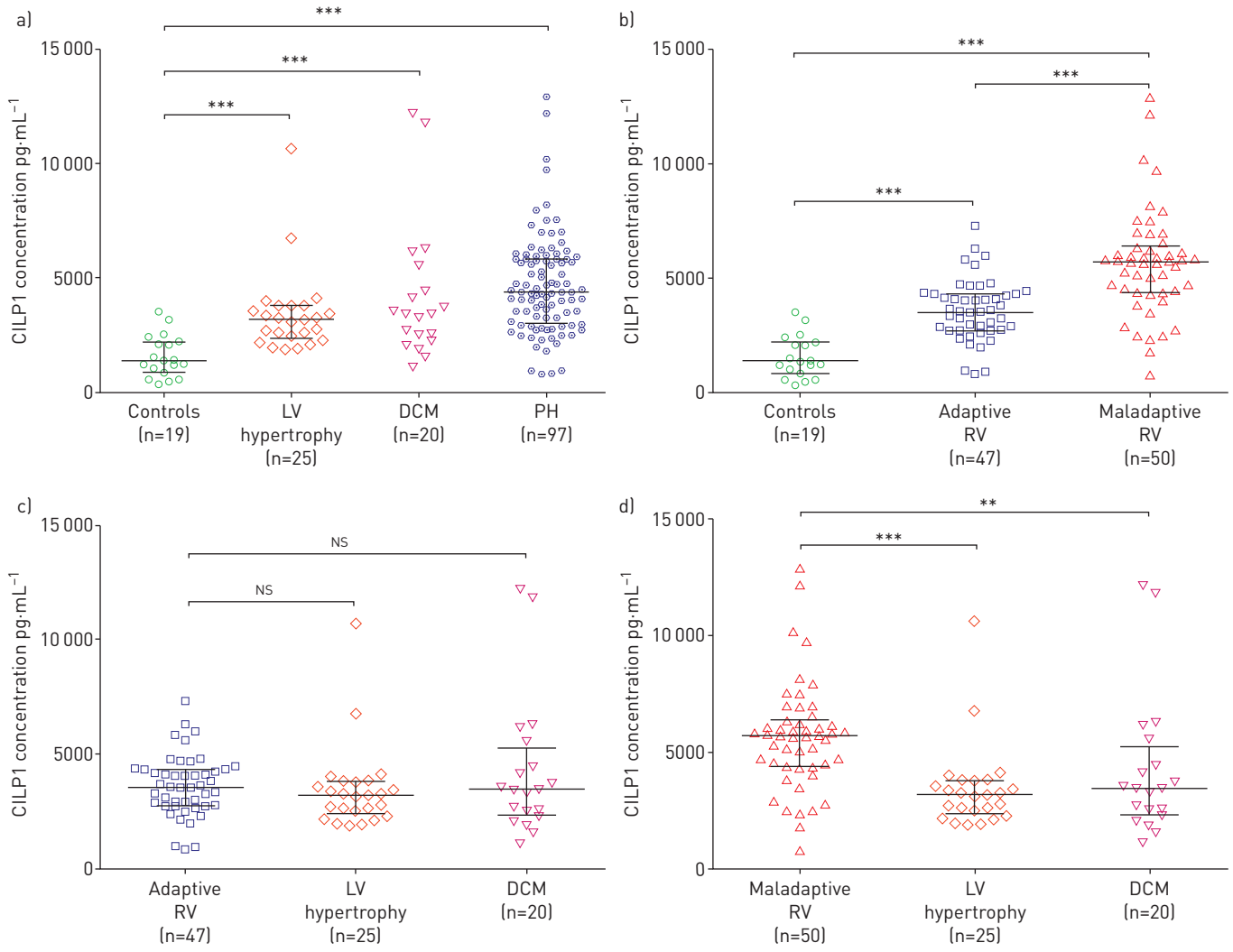

FIGURE 3 Box and scatter plots comparing serum cartilage intermediate layer protein 1 (CILP1) concentrations. a) Left ventricular (LV) hypertrophy, dilative cardiomyopathy (DCM), pulmonary hypertension (PH) and controls; b) adaptive or maladaptive right ventricle (RV) and controls; c) adaptive RV, LV hypertrophy and DCM; d) maladaptive RV, LV hypertrophy and DCM. Boxes represent median and interquartile range. NS: nonsignificant. **: p<0.01, ***: p<0.001.

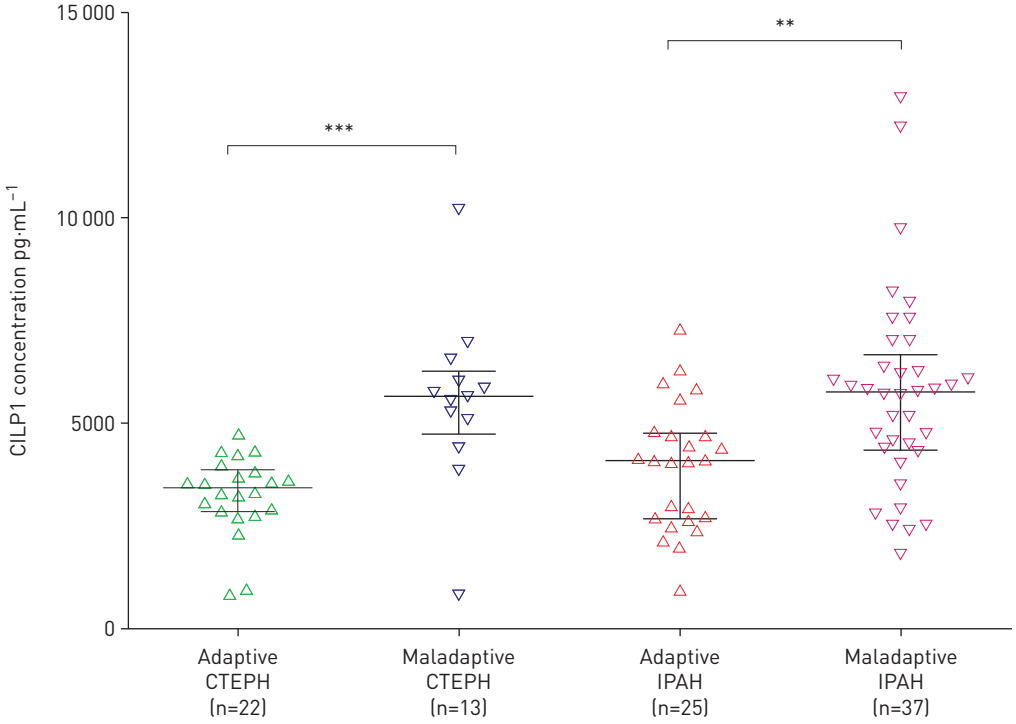

FIGURE 4 Box and scatter plots comparing serum cartilage intermediate layer protein (CILP)1 concentrations in right ventricle subgroups. Shown are values for adaptive and maladaptive chronic thromboembolic pulmonary hypertension (CTEPH) as well as adaptive and maladaptive idiopathic pulmonary arterial hypertension (IPAH). Boxes represent median and interquartile range. *: p<0.05, ***: p<0.001.

maladaptive CTEPH and IPAH patients (figure 4). There was no difference between adaptive CTEPH and adaptive IPAH (p=0.16) and maladaptive CTEPH and maladaptive IPAH (p=0.85).

The median NT-proBNP concentrations in patients with adaptive and maladaptive RV, LV hypertrophy and DCM are given in table 2 and shown in greater detail in figure 5. NT-proBNP concentrations were significantly higher in the maladaptive group than in the adaptive group, but there were no differences between the maladaptive RV group and the LV groups (figure 5). The adaptive RV group showed lower NT-proBNP concentrations than the DCM group and there was no difference as compared with the LV hypertrophy group (figure 5).

CILP1 as predictor of maladaptive RV

ROC curve analysis in all PH patients showed that both CILP1 and NT-proBNP are good predictors of maladaptive RV (figure 6). There was no significant difference between the two ROC curves (p=0.4).

An optimal CILP1 cut-off value of 4373 pg·mL^{-1} was determined. The clinical and diagnostic characteristics of PH patients with low CILP1 (4373 pg·mL^{-1}; n=48) and high CILP1 (⩾4373 pg·mL^{-1}; n=49) are shown in table 3. The TAPSE/PASP ratio showed the strongest association with high CILP1 (figure 7a). High CILP1 was also associated with significantly higher NT-proBNP levels (figure 8).

TAPSE/PASP ratios were divided into three groups according to their tertiles: low (TAPSE/PASP <0.15 mm·mmHg^{-1}), middle (TAPSE/PASP 0.15–0.33 mm·mmHg^{-1}) and high (TAPSE/PASP >0.33 mm·mmHg^{-1}). CILP1 concentrations were higher in the low tertile as compared with the middle and the high tertiles (figure 7b). There were no significant differences in CILP1 concentrations between the middle and high tertiles.

In a logistic regression model adjusted for the three parameters that showed the strongest association with high CILP1, TAPSE/PASP, mean PAP and RVD, TAPSE/PASP was the only independent predictor of high CILP1 (supplementary table S1)

Discussion

The present study is the first to assess CILP1 protein levels in the RV myocardium in an experimental model of RV pressure overload and serum CILP1 concentrations in humans with adaptive and maladaptive PH, LV hypertrophy and DCM. The main findings of this study are 1) the amount of CILP1

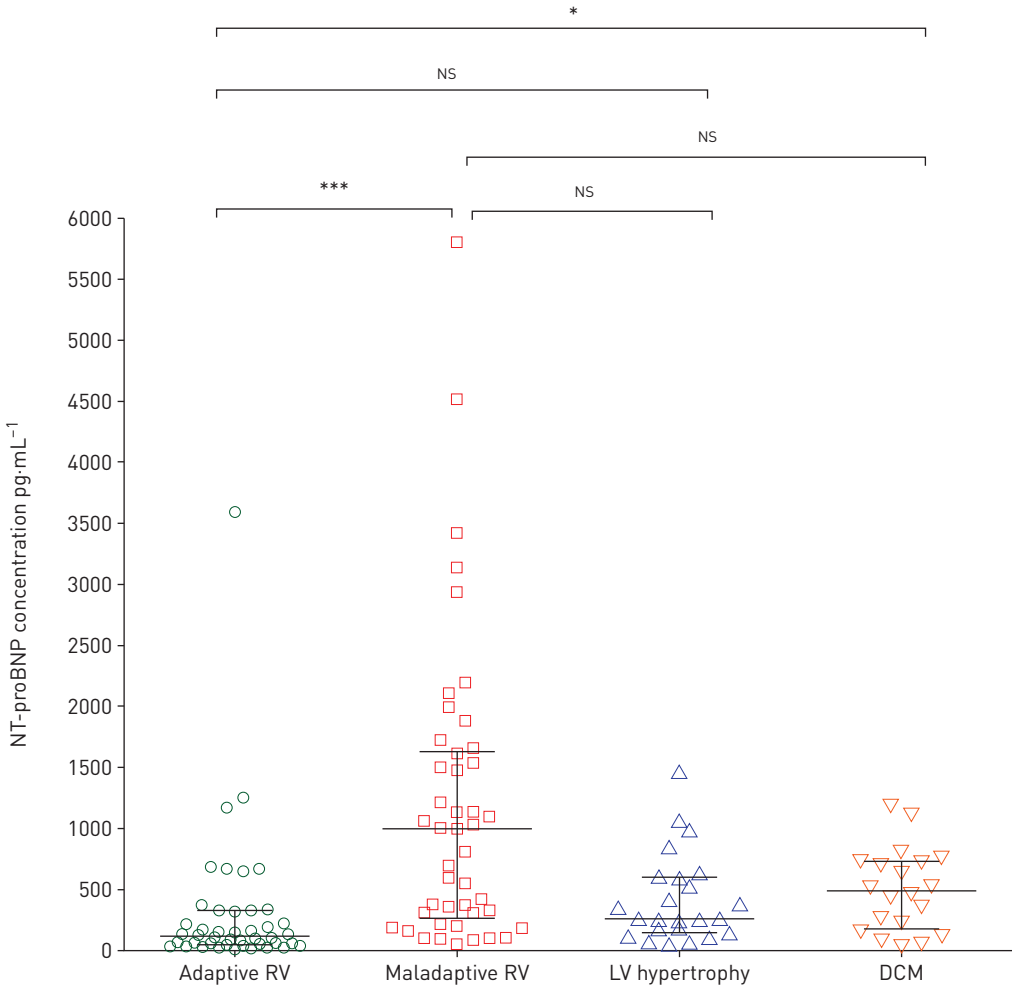

FIGURE 5 Box and scatter plots comparing serum N-terminal pro-brain natriuretic peptide (NT-proBNP) concentrations. Shown are values for adaptive and maladaptive right ventricle (RV), left ventricular (LV) hypertrophy and dilative cardiomyopathy (DCM). Boxes represent median and interquartile range. NS: nonsignificant. *: p<0.05, ***: p<0.001.

protein in the murine RV is higher after severe PAB than after sham treatment; 2) CILP1 expression in human cardiac fibroblasts shows an early and strong increase under TGF-β1 stimulation; 3) concentrations in patients with PH, LV hypertrophy or DCM are higher than in patients without LV or RV abnormalities; 4) high CILP1 concentrations are associated with maladaptive RV function in PH; and 5) CILP1 concentrations in maladaptive PH are higher than in LV hypertrophy and DCM.

CILP1 as a biomarker of cardiac remodelling

The family of TGF-β comprises cytokines that activate profibrotic signalling pathways in myocardium by inducing expression of ECM proteins and promoting myofibroblast transdifferentiation [14]. CILP1 is an ECM protein that was identified as an antagonist of TGF-β signalling [6], and its expression is induced by TGF-β [15]. Recent studies demonstrated that CILP1 is expressed in human myocardium, where it is primarily produced by cardiac fibroblasts [6].

In our study, TGF-β1 treatment also induced a significant increase in CILP1 transcript levels as early as 6 h in human cardiac fibroblasts. In contrast to the transcriptional activation of CILP1 gene upon TGF-β1 treatment, serum-supplemented culture conditions significantly repressed CILP1 transcription in human cardiac fibroblasts at all time points, which corroborates with the findings in rat cardiac fibroblasts [6]. When compared to the stably maintained CILP1 expression levels from 6 h, the TGF-β1-induced transcriptional responses from other cardiac ECM-related genes were relatively slower, with statistically significant transcriptional changes detectable in POSTN and FN1 genes and a trend towards higher COL1A2 levels only at 72 h. Importantly, the significantly elevated transcript levels of CILP1 observed at 72 h correlated with the increased transcription of key profibrotic mediators such as POSTN, FN1 and

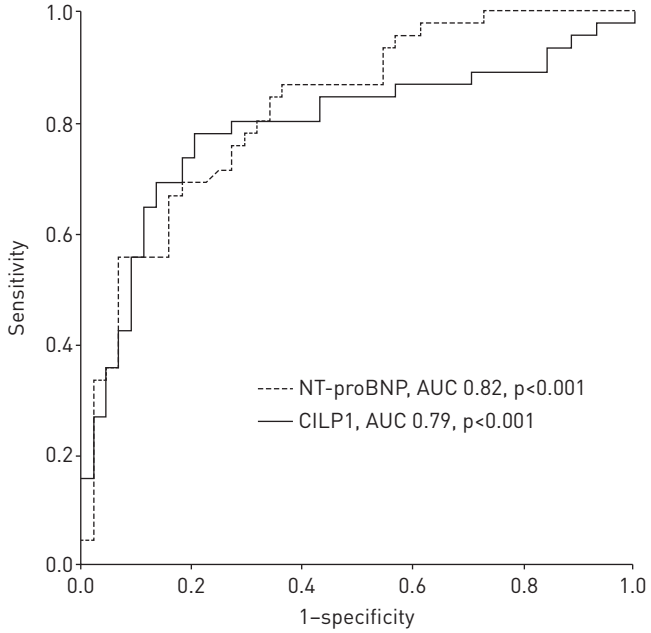

FIGURE 6 Receiver operating characteristics curve showing the predictive power of cartilage intermediate layer protein (CILP)1 and N-terminal pro-brain natriuretic peptide (NT-proBNP) for maladaptive right ventricle. AUC: area under the curve.

TABLE 3 Clinical characteristics of patients grouped according to cartilage intermediate layer protein (CILP)1 cut-off value

	CILP1 <4373 pg·mL^{-1}	CILP1 ⩾4373 pg·mL^{-1}	p-value
Patients	48	49	
Female	26 (54)	27 (55)	0.92
Age years	62 (50–69)	62 (49–71)	0.95
BMI kg·m^{-2}	28 (24–32)	26 (23–30)	0.24
CAD	20 (65)	22 (69)	0.38
NYHA class ⩾III	9 (19)	12 (25)	0.72
Diabetes	13 (27)	11 (23)	0.63
Right heart catheterisation			
PASP mmHg	64 (52–82)	88 (67–95)	0.001
Mean PAP mmHg	41 (33–52)	55 (42–59)	0.001
Cardiac index L·min^{-1}·m^{-2}	2.79 (2.05–3.21)	1.95 (1.56–2.31)	0.01
Mean PAWP mmHg	10 (7–12)	9 (8–11)	0.68
RAP mmHg	6 (5–10)	10 (7–13)	0.003
Echocardiography			
TAPSE mm	21 (20–25)	15 (12–20)	<0.0001
LVEF	63 (60–67)	62 (60–70)	0.88
RVD mm	42 (35–47)	48 (44–52)	<0.001
IVSd mm	10 (9–11)	10 (9–11)	0.25
LVPWd mm	9 (8–11)	10 (9–11)	0.49
TAPSE/PASP mm·mmHg^{-1}	0.34 (0.26–0.47)	0.17 (0.14–0.24)	<0.0001
CILP1 pg·mL^{-1}	3034 (2494–3916)	5828 (5152–6550)	<0.0001
NT-proBNP pg·mL^{-1}	195 (83–639)	647 (182–1478)	<0.01

Data are presented as n, n (%) or median (interquartile range). BMI: body mass index; CAD: coronary artery disease; NYHA: New York Heart Association; PASP: pulmonary arterial systolic pressure; PAP: pulmonary artery pressure; PAWP: pulmonary artery wedge pressure; RAP: right atrial pressure; TAPSE: tricuspid annular plane systolic excursion; LVEF: left ventricular ejection fraction; RVD: right ventricular diameter; IVSd: diastolic interventricular septum thickness; LVPWd: diastolic left ventricular posterior wall thickness; NT-proBNP: N-terminal pro-brain natriuretic peptide.

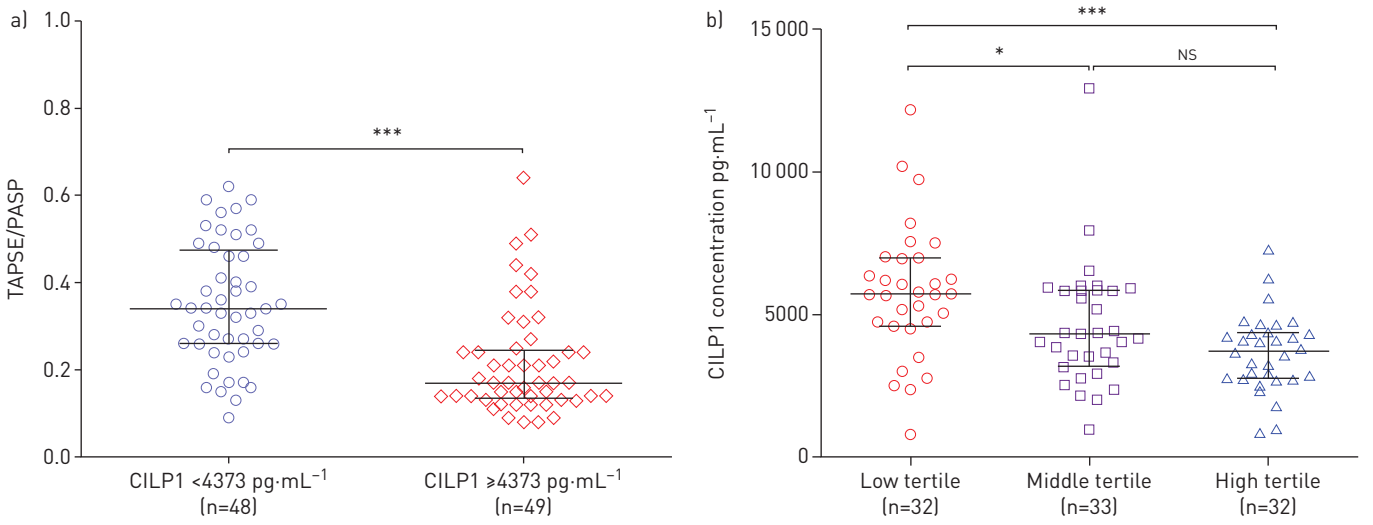

FIGURE 7 Box and scatter plots comparing a) tricuspid annular plane systolic excursion (TAPSE)/pulmonary arterial systolic pressure (PASP) values according to cartilage intermediate layer protein (CILP)1 cut-off and b) CILP1 concentrations according to the TAPSE/PASP tertiles (low tertile: TAPSE/PASP <0.15 mm·mmHg^{-1}; middle tertile: TAPSE/PASP 0.15–0.33 mm·mmHg^{-1}; high tertile: TAPSE/PASP >0.33 mm·mmHg^{-1}) in pulmonary hypertension patients. NS: nonsignificant. *: p<0.05, ***: p<0.001.

COL1A2. Overall, CILP1 is a potential early cellular marker for TGF-β1-induced fibrotic responses in human cardiac fibroblasts that displayed significant correlation with other integral components of cardiac ECM that are frequently implicated in cardiac fibrosis.

Expression analysis in several different mouse models of cardiac remodelling, including transverse aortic constriction and angiotensin infusion detected a marked upregulation of CILP1 expression that was also highly correlated with the expression of TGF-β and other ECM proteins. Furthermore, microarray analysis of endomyocardial biopsies in patients with aortic stenosis and of human infarct tissue showed elevated CILP1 expression [6]. These findings suggest that TGF-β and CILP1 may form a functional feedback loop that plays an important role in the pathogenesis of cardiac fibrosis.

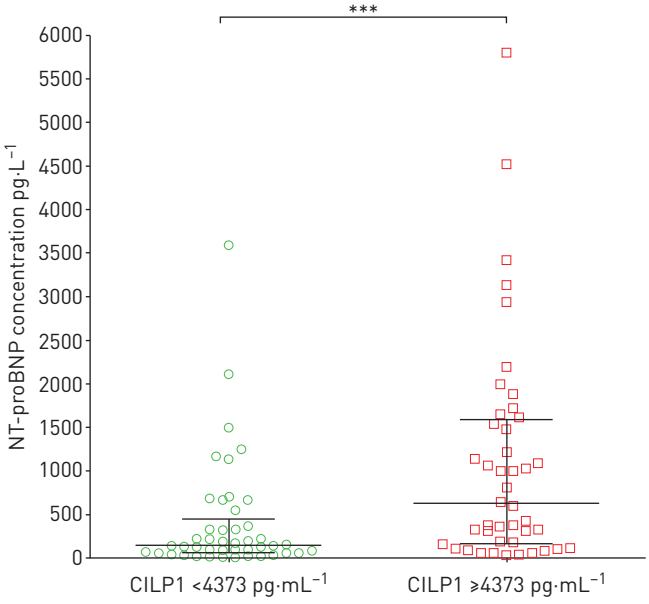

FIGURE 8 Box and scatter plots comparing serum N-terminal pro-brain natriuretic peptide (NT-proBNP) concentrations according to cartilage intermediate layer protein 1 (CILP1) cut-off value. Shown are values for CILP1 <4373 pg·mL^{-1} and CILP1 ⩾4373 pg·mL^{-1}. Boxes represent median and interquartile range. ***: p<0.001.

In our study CILP1 serum concentrations were significantly increased in all groups with LV or RV abnormalities. These findings suggest that CILP1 could be a novel biomarker of pathological cardiac remodelling and specifically of cardiac fibrosis because of its involvement in fibrotic signalling.

Aetiology of RV adaptation and maladaptation in PH

In PH, vascular remodelling leads to an increase in pulmonary vascular resistance, which subsequently causes a markedly higher RV afterload. Initially, adaptive RV changes such as hypertrophy and optimised intrinsic contractile properties result in enhanced contractility. Thus, normal stroke volume is maintained despite the higher vascular load (ventriculoarterial coupling) [16]. However, progressive RV pressure overload leads to increased wall stress and neurohumoral activation, which triggers maladaptive RV remodelling associated with dilation, capillary rarefication, metabolic dysfunction, fibrosis and diastolic stiffness [17]. Finally, ventriculoarterial uncoupling occurs with reduced output and right heart failure.

Diastolic stiffness and fibrosis appear to be prognostically important signs of maladaptation. Several studies have shown a connection between diastolic stiffness, fibrosis and maladaptation. Diastolic stiffness was characterised by increased fibrosis and intrinsic stiffening of the RV cardiomyocyte sarcomeres and was closely associated with PH disease severity [18]. It was also associated with worse prognosis in pulmonary arterial hypertension patients [19]. Recent histological and cardiac imaging studies have demonstrated increased RV fibrosis in patients with end-stage PH and RV failure [20–23].

Recent studies involving cardiac magnetic resonance strain and pressure–volume loop measurements show that the loss of lusitropic function through RV stiffening may be a crucial event which, together with other maladaptive processes such as RV dilation, leads to heart failure [18, 24]. In our study the amount of collagen types I and III, which are the main structural collagens of the myocardial ECM [25], was significantly increased in mice given severe PAB as compared to sham. This also indicates an increased RV fibrosis during RV pressure overload. Taken together, these findings suggest that biomarkers that specifically indicate RV fibrosis may correlate with maladaptive RV changes and could help to better identify patients with a high risk of right heart failure and worse outcomes.

CILP1 as a biomarker of RV maladaptation and fibrosis

The precise definition of maladaptive RV remains controversial, and there are currently no established diagnostic standards of RV maladaptation. Current research is focused on identifying a set of diagnostic tools that could detect the complex functional and structural changes that occur during this pathological process. A combination of clinical, imaging and biochemical parameters could thus allow a more accurate risk stratification and prediction of outcomes. As mentioned above, RV fibrosis appears to be an important pathological feature of maladaptive RV and right heart failure.

In our study, patients were assigned to the maladaptive group according to functional and structural criteria such as low TAPSE, low cardiac index and RV dilatation that are typical of patients with right heart failure. In addition, maladaptive RV patients showed a low TAPSE/PASP ratio, which is a novel method of measuring RV contractility and ventriculoarterial coupling noninvasively [26, 27]. It has been validated as an important clinical and prognostic parameter in PH patients with right heart failure [28–30]. In our analysis, TAPSE/PASP was the only independent predictor of high CILP1 concentrations, and CILP1 concentrations in the low TAPSE/PASP tertile (<0.16 mm·mmHg^{-1}) were higher than in the other tertiles. In a study by Tello *et al.* [30], PAH patients were grouped according to their TAPSE/PASP ratios in tertiles that were very similar to those in our analysis. Patients in the low tertile (<0.19 mm·mmHg^{-1}) showed significantly compromised functional status and higher mortality compared with patients in the middle (0.19–0.32 mm·mmHg^{-1}) and high (>0.32 mm·mmHg^{-1}) tertiles. Furthermore, CILP1 was a good predictor of maladaptive RV in ROC analysis and high CILP1 levels were associated with significantly lower TAPSE/PASP ratios.

NT-proBNP is the only established biomarker in the various settings of PH. Higher NT-proBNP levels are associated with myocardial dysfunction and worse prognosis [3, 31, 32]. The most recent guidelines on PH recommend routine measurements of NT-proBNP at the time of diagnosis of PH and during follow-up [33]. However, NT-proBNP is not specific and can be elevated in almost any heart disease [33].

Accordingly, NT-proBNP was associated with maladaptive RV function in our study. Notably, a direct comparison between the AUCs of CILP1 and NT-proBNP revealed that CILP1 performed as well as NT-proBNP as a predictor of maladaptive RV. NT-proBNP was also associated with high CILP1 concentrations.

Our findings suggest that high CILP1 is associated with RV maladaptation, ventriculoarterial uncoupling and right heart failure. Thus, CILP1 may be a novel biomarker of RV maladaptation and fibrosis that is associated with worse prognosis.

Furthermore, our analysis shows that patients with maladaptive RV exhibited higher CILP1 concentrations than patients with LV hypertrophy and DCM. The hypothesis that CILP1 expression is higher with RV pressure overload than with LV pressure overload is further supported by an experimental study revealing a 26-fold upregulation of CILP1 in mice with pulmonary artery constriction and only a five-fold upregulation in mice subjected to transverse aortic constriction, despite a similar degree of outflow tract obstruction [8]. Although RV pressure overload also leads to increased RV fibrosis, LV fibrosis in DCM is usually much more pronounced [34]. The CILP1 pathway could be involved in preventing excessive fibrosis by inhibiting profibrotic TGF-β signalling in the myocardium. Therefore, a weaker upregulation of CILP1 expression could explain the more pronounced LV fibrosis. Thus, if different CILP1 cut-offs were used, CILP1 could function as a biomarker of pathological cardiac remodelling that is able to differentiate between LV and RV disease.

Limitations

No haemodynamic measurements were performed in the operated animals; thus, PAB severity and the resulting RV pressure overload cannot be exactly assessed. This limits the validity of our experimental analysis.

Molecular analyses in the experimental animals and in the human cardiac fibroblasts only show an indirect association of CILP and myocardial fibrosis. Furthermore, no data was obtained on myocardial fibrosis after mild PAB.

The clinical data represent a single-centre study of observational nature. The sample size was small, which could limit the validity of our analyses. Nevertheless, this proof-of-concept study clearly demonstrates a significant increase in CILP1 concentration in patients with LV and RV pressure overload and an association of CILP1 with maladaptive RV function.

Conclusion

Our analysis demonstrates the potential role of CILP1 as a novel biomarker of RV and LV pathological remodelling that is associated with RV maladaptation and ventriculoarterial uncoupling in the setting of pulmonary hypertension. Further research is needed to validate these findings and explore the biomolecular mechanisms responsible for a potentially differential CILP1 expression in RV and LV.

Acknowledgement: We acknowledge the expertise of Elizabeth Martinson of the KHFI Editorial Office (Bad Nauheim, Germany) in preparing the manuscript.

Conflict of interest: S. Keranov reports grants from German Research Foundation (Project B07, Collaborative Research Center 1213-Pulmonary Hypertension and Cor Pulmonale), during the conduct of the study. O. Dörr reports grants from German Research Foundation (Project B07, Collaborative Research Center 1213-Pulmonary Hypertension and Cor Pulmonale), during the conduct of the study. L. Jafari has nothing to disclose. C. Troidl has nothing to disclose. C. Liebetrau reports grants from German Research Foundation (Project B07, Collaborative Research Center 1213-Pulmonary Hypertension and Cor Pulmonale), during the conduct of the study. S. Kriechbaum reports grants from German Research Foundation (Project B07, Collaborative Research Center 1213-Pulmonary Hypertension and Cor Pulmonale), during the conduct of the study. T. Keller has nothing to disclose. S. Voss has nothing to disclose. T. Bauer has nothing to disclose. J. Lorenz has nothing to disclose. M.J. Richter has nothing to disclose. K. Tello has nothing to disclose. H. Gall has nothing to disclose. H.A. Ghofrani has nothing to disclose. E. Mayer has nothing to disclose. C.B. Wiedenroth has nothing to disclose. S. Guth has nothing to disclose. H. Lörchner has nothing to disclose. J. Pöling has nothing to disclose. P. Chelladurai has nothing to disclose. S.S. Pullamsetti has nothing to disclose. T. Braun has nothing to disclose. W. Seeger has nothing to disclose. C.W. Hamm reports grants from German Research Foundation (Project B07, Collaborative Research Center 1213-Pulmonary Hypertension and Cor Pulmonale), during the conduct of the study. H. Nef reports grants from German Research Foundation (Project B07, Collaborative Research Center 1213-Pulmonary Hypertension and Cor Pulmonale), during the conduct of the study.

Support statement: This work was supported by Project B07, Collaborative Research Center 1213-Pulmonary Hypertension and Cor Pulmonale, German Research Foundation (DFG).

References

1 Naeije R, Manes A. The right ventricle in pulmonary arterial hypertension. *Eur Respir Rev* 2014; 23: 476–487.
2 Campo A, Mathai SC, Le Pavec J, *et al.* Outcomes of hospitalisation for right heart failure in pulmonary arterial hypertension. *Eur Respir J* 2011; 38: 359–367.
3 Fijalkowska A, Kurzyna M, Torbicki A, *et al.* Serum N-terminal brain natriuretic peptide as a prognostic parameter in patients with pulmonary hypertension. *Chest* 2006; 129: 1313–1321.
4 Heresi GA, Tang WH, Aytekin M, *et al.* Sensitive cardiac troponin I predicts poor outcomes in pulmonary arterial hypertension. *Eur Respir J* 2012; 39: 939–944.
5 Rhodes CJ, Wharton J, Ghataorhe P, *et al.* Plasma proteome analysis in patients with pulmonary arterial hypertension: an observational cohort study. *Lancet Respir Med* 2017; 5: 717–726.
6 van Nieuwenhoven FA, Munts C, Op't Veld RC, *et al.* Cartilage intermediate layer protein 1 (CILP1): a novel mediator of cardiac extracellular matrix remodelling. *Sci Rep* 2017; 7: 16042.

7 Smeets PJ, de Vogel-van den Bosch HM, Willemsen PH, *et al.* Transcriptomic analysis of PPARα-dependent alterations during cardiac hypertrophy. *Physiol Genomics* 2008; 36: 15–23.
8 Kreymborg K, Uchida S, Gellert P, *et al.* Identification of right heart-enriched genes in a murine model of chronic outflow tract obstruction. *J Mol Cell Cardiol* 2010; 49: 598–605.
9 Lörchner H, Pöling J, Gajawada P, *et al.* Myocardial healing requires Reg3β-dependent accumulation of macrophages in the ischemic heart. *Nat Med* 2015; 21: 353–362.
10 Polyakova V, Richter M, Ganceva N, *et al.* Distinct structural and molecular features of the myocardial extracellular matrix remodeling in compensated and decompensated cardiac hypertrophy due to aortic stenosis. *IJC Heart Vessels* 2014; 4: 145–160.
11 Gall H, Felix JF, Schneck FK, *et al.* The Giessen Pulmonary Hypertension Registry: survival in pulmonary hypertension subgroups. *J Heart Lung Transplant* 2017; 36: 957–967.
12 Lang RM, Badano LP, Mor-Avi V, *et al.* Recommendations for Cardiac Chamber Quantification by Echocardiography in Adults: an update from the American Society of Echocardiography and the European Association of Cardiovascular Imaging. *Eur Heart J Cardiovasc Imaging* 2015; 16: 233–270.
13 Rosenkranz S, Preston IR. Right heart catheterisation: best practice and pitfalls in pulmonary hypertension. *Eur Respir Rev* 2015; 24: 642–652.
14 Biernacka A, Dobaczewski M, Frangogiannis NG. TGF-beta signaling in fibrosis. *Growth Factors* 2011; 29: 196–202.
15 Mori M, Nakajima M, Mikami Y, *et al.* Transcriptional regulation of the cartilage intermediate layer protein (CILP) gene. *Biochem Biophys Res Commun* 2006; 341: 121–127.
16 Vonk Noordegraaf A, Westerhof BE, Westerhof N. The relationship between the right ventricle and its load in pulmonary hypertension. *J Am Coll Cardiol* 2017; 69: 236–243.
17 van der Bruggen CEE, Tedford RJ, Handoko ML, *et al.* RV pressure overload: from hypertrophy to failure. *Cardiovasc Res* 2017; 113: 1423–1432.
18 Rain S, Handoko ML, Trip P, *et al.* Right ventricular diastolic impairment in patients with pulmonary arterial hypertension. *Circulation* 2013; 128: 2016–2025.
19 Trip P, Rain S, Handoko ML, *et al.* Clinical relevance of right ventricular diastolic stiffness in pulmonary hypertension. *Eur Respir J* 2015; 45: 1603–1612.
20 Freed BH, Gomberg-Maitland M, Chandra S, *et al.* Late gadolinium enhancement cardiovascular magnetic resonance predicts clinical worsening in patients with pulmonary hypertension. *J Cardiovasc Magn Reson* 2012; 14: 11.
21 Ozawa K, Funabashi N, Takaoka H, *et al.* Detection of right ventricular myocardial fibrosis using quantitative CT attenuation of the right ventricular myocardium in the late phase on 320 slice CT in subjects with pulmonary hypertension. *Int J Cardiol* 2017; 228: 165–168.
22 Drake JI, Bogaard HJ, Mizuno S, *et al.* Molecular signature of a right heart failure program in chronic severe pulmonary hypertension. *Am J Respir Cell Mol Biol* 2011; 45: 1239–1247.
23 Frangogiannis NG. Fibroblasts and the extracellular matrix in right ventricular disease. *Cardiovasc Res* 2017; 113: 1453–1464.
24 Tello K, Dalmer A, Vanderpool R, *et al.* Cardiac magnetic resonance imaging-based right ventricular strain analysis for assessment of coupling and diastolic function in pulmonary hypertension. *JACC Cardiovasc Imaging* 2019; 12: 2155–2164.
25 Gyöngyösi M, Winkler J, Ramos I, *et al.* Myocardial fibrosis: biomedical research from bench to bedside. *Eur J Heart Fail* 2017; 19: 177–191.
26 Guazzi M, Bandera F, Pelissero G, *et al.* Tricuspid annular plane systolic excursion and pulmonary arterial systolic pressure relationship in heart failure: an index of right ventricular contractile function and prognosis. *Am J Physiol Heart Circ Physiol* 2013; 305: H1373–H1381.
27 Guazzi M, Dixon D, Labate V, *et al.* RV contractile function and its coupling to pulmonary circulation in heart failure with preserved ejection fraction: stratification of clinical phenotypes and outcomes. *JACC Cardiovasc Imaging* 2017; 10: 1211–1221.
28 Guazzi M, Villani S, Generati G, *et al.* Right ventricular contractile reserve and pulmonary circulation uncoupling during exercise challenge in heart failure: pathophysiology and clinical phenotypes. *JACC Heart Fail* 2016; 4: 625–635.
29 Guazzi M, Naeije R, Arena R, *et al.* Echocardiography of right ventriculoarterial coupling combined with cardiopulmonary exercise testing to predict outcome in heart failure. *Chest* 2015; 148: 226–234.
30 Tello K, Axmann J, Ghofrani HA, *et al.* Relevance of the TAPSE/PASP ratio in pulmonary arterial hypertension. *Int J Cardiol* 2018; 266: 229–235.
31 Leuchte HH, El Nounou M, Tuerpe JC, *et al.* N-terminal pro-brain natriuretic peptide and renal insufficiency as predictors of mortality in pulmonary hypertension. *Chest* 2007; 131: 402–409.
32 Fritz JS, Blair C, Oudiz RJ, *et al.* Baseline and follow-up 6-min walk distance and brain natriuretic peptide predict 2-year mortality in pulmonary arterial hypertension. *Chest* 2013; 143: 315–323.
33 Galiè N, Humbert M, Vachiery JL, *et al.* 2015 ESC/ERS Guidelines for the diagnosis and treatment of pulmonary hypertension: The Joint Task Force for the Diagnosis and Treatment of Pulmonary Hypertension of the European Society of Cardiology (ESC) and the European Respiratory Society (ERS): Endorsed by: Association for European Paediatric and Congenital Cardiology (AEPC), International Society for Heart and Lung Transplantation (ISHLT). *Eur Heart J* 2016; 37: 67–119.
34 Aoki T, Fukumoto Y, Sugimura K, *et al.* Prognostic impact of myocardial interstitial fibrosis in non-ischemic heart failure. Comparison between preserved and reduced ejection fraction heart failure. *Circ J* 2011; 75: 2605–2613.